PHYSICAL REVIEW C VOLUME 26, NUMBER 5 NOVEMBER 1982

Mechanisms of heavy ion dissipative collisions: The $^{209}Bi+^{84}Kr$ reaction at $E_{lab}=712$ MeV

J. R. Birkelund, H. Freiesleben,* J. R. Huizenga, W. U. Schröder, and W. W. Wilcke
Departments of Chemistry and Physics and Nuclear Structure Research Laboratory, University of Rochester, Rochester, New York 14627

K. L. Wolf and J. P. Unik
Chemistry Division, Argonne National Laboratory, Argonne, Illinois 60439

V. E. Viola, Jr.†
Chemistry Department, University of Maryland, College Park, Maryland 20742
(Received 19 July 1982)

Projectilelike reaction products from the $^{209}Bi+^{84}Kr$ reaction were studied at a laboratory bombarding energy of 712 MeV. The fragments were identified by atomic number, and their kinetic energies and angular distributions were measured with solid-state ΔE-E telescopes. The angular distribution is found to be peaked at an angle slightly smaller than the grazing angle and the Z distribution is peaked near $Z=36$. Correlations of the experimental variables show that the angular and Z distributions broaden drastically with kinetic energy dissipation in damped reactions. Various correlations between experimental observables, including the variance of the Z distributions as a function of the reaction Q value and the relationship between kinetic energy and reaction angle, are interpreted in terms of a classical dynamical model using a proximity one-body transport formalism.

[NUCLEAR REACTIONS $^{209}Bi(^{84}Kr,HI)$; $E_{lab}=712$ MeV; measured $\sigma(\theta,E,Z)$; damped reaction; extracted moments of element distributions and centroids of angular distributions as a function of Q value; comparison with dynamical calculations employing proximity one-body transport model.]

I. INTRODUCTION

The study of nuclear interactions between very heavy target and projectile nuclei has contributed much to the understanding of the gross features of the damped reaction mechanism. Such collisions are also described as dissipative or deep-inelastic heavy-ion reactions. The unique properties of damped reactions are derived from an irreversible transmutation of a significant fraction of the initial kinetic energy of relative motion and the exchange of a large number of nucleons between the reaction partners. Rather high excitation energies attained during a reaction and multiple-particle exchange processes observed have led to the introduction of transport theories for a description of the microscopic events taking place in a damped heavy-ion collision. On the other hand, a satisfactory understanding of the basic principles of the reaction mechanism has as yet not been achieved. For example, models emphasizing collective modes of nuclear excitation rather than transport mechanisms are also often invoked in the discussion of the dissipative features of heavy-ion reactions. A clear distinction between such controversial views of the microscopic reaction mechanism on the basis of experimental data can apparently only be gained through a systematical comparison of model predictions with the various correlations between reaction variables observed experimentally. Comparisons involving models based on a minimum of free parameters and capable of yielding estimates for many observables simultaneously are, obviously, most instructive for an exploration of the damped reaction mechanism. Thus far, only a limited number of detailed studies of the properties of energy dissipation and mass exchange have been reported.

The main purpose of this work is to discuss the

implications of experimental correlations between energy dissipation, charge exchange, and collective motion in the reaction $^{209}Bi + ^{84}Kr$ at $E_{lab} = 712$ MeV. Comparisons will be made between experimental data and the predictions of a transport model emphasizing the exchange of independent nucleons between the reaction partners as the dominant origin of all transport phenomena in nuclear reactions. Apart from the adoption of a family of shapes for the intermediate dinuclear system and approximations in the calculation of the Coulomb interaction potential, there are no free parameters in the model; hence, it possesses an outstanding predictive power. In addition, for illustrative purposes, the data are compared also to a simplified version of the model.

The reaction $^{209}Bi + ^{84}Kr$ was chosen for this study because it involves a rather heavy system where the reaction is expected to be dominated by the strong Coulomb repulsion and where, hence, a large number of partial waves contribute to the damped process. Also, the availability of data for this system[1,2] at several incident energies is regarded as essential for a systematic test of frictional forces predicted by theory. In addition, the opportunity is taken to present correlation data for the $^{209}Bi + ^{84}Kr$ reaction, at $E_{lab} = 712$ MeV, that have not been available in the literature (except for a few selected results reported in a short communication[3] and at conferences[4–6]), although reference to this reaction has frequently been made in other work.[7–14]

Therefore, the following section presents a brief description of the experimental methods and procedures used in obtaining the data, while in Sec. III fragment angular and atomic-number distributions, as well as their correlations with the amount of dissipated energy, are discussed. Model interpretations of the experimental results are discussed in Sec. IV.

II. EXPERIMENTAL PROCEDURE

The measurements were performed at the Lawrence Berkeley Laboratory SuperHILAC accelerator with ^{84}Kr projectiles of 600 and 712 MeV. Elemental bismuth targets with dimensions of 3×6 mm were prepared by vacuum evaporation onto 100 $\mu g/cm^2$ carbon backing foils. Target material thicknesses were in most cases between 100–200 $\mu g/cm^2$.

The reaction products were studied with silicon surface-barrier detector systems. In addition to a single detector subtending an angle of 0.5° in the reaction plane, a second system, used for charge identification in addition to energy determination, consisted of a ΔE-E telescope with a 12-μm silicon transmission counter and a 60-μm stopping detector. An 8×50 mm position-sensitive surface barrier detector was used to measure the energy and angle of products in coincidence with either of the other two detector systems. Beam monitor detectors consisted of two silicon surface barrier detectors mounted at $\pm 25°$ from the beam and 15° above the reaction plane. Counts in the monitor detectors were used to determine left-right changes in beam direction and for cross section normalization.

All data were collected event by event in singles and coincidence modes. Signals from a pulse generator triggered by monitor detectors were fed into the detector preamplifier during the beam pulses. The system live time was obtained by comparing the counts in the pulser peak in the recorded pulse spectrum with the number of pulses counted by an ungated scaler connected directly to the pulse generator.

The cross section for elastic scattering of ^{84}Kr on ^{209}Bi was measured as a function of angle. Experimental results and a detailed theoretical analysis have been published previously.[15] The full width at half maximum (FWHM) of the elastic peak corresponds to an energy resolution of approximately 1.5% for the silicon telescope. At angles in the vicinity of the quarter-point angle ($\sigma_{el}/\sigma_{Ruth} = 0.25$), the elastic events were separated from the inelastic or damped events by fitting an experimental standard elastic peak, associated with a more forward angle, to these data. This fitting procedure is illustrated for the $^{209}Bi + ^{84}Kr$ ($E_{lab} = 712$ MeV) data elsewhere.[15] Such experiments are, of course, incapable of resolving low-lying inelastic excitations as shown by a recent high-resolution study.[16] The Z resolution (FWHM) of the ΔE-E telescope as determined from elastic scattering of the ^{84}Kr was approximately 2 units.

III. RESULTS AND DISCUSSION

In this section two types of experimental distributions will be illustrated. First the simple, one-dimensional experimental distributions will be discussed. These will be followed by more detailed correlations of the experimental data.

A. Simple experimental distributions

Reaction products formed in dissipative collisions between heavy ions have characteristic types of angular, charge, and energy distributions.[17] The ex-

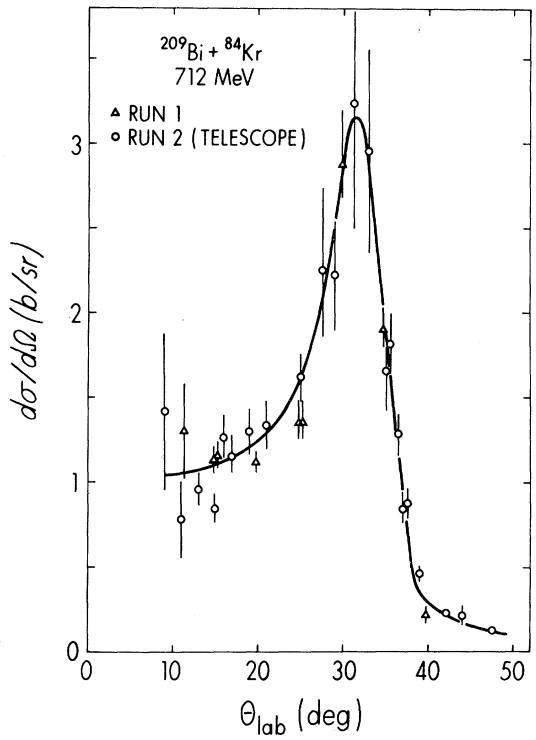

FIG. 1. Laboratory angular distribution of light (Kr-like) reaction products.

perimental angular distribution for all damped reaction products from the ^{209}Bi + ^{84}Kr reaction at a bombarding energy of 712 MeV is shown in Fig. 1. The differential cross section is seen to be peaked at an angle of approximately 31° in the laboratory frame, somewhat forward of the grazing angle of 34°. This strong sideways peaking, or "angular focusing," is a feature characteristic of very heavy ion collisions a few MeV per nucleon above the Coulomb barrier. For ^{209}Bi + ^{84}Kr at 712 MeV,

$$[(E_{\text{c.m.}} - V_C)/\mu \approx 3.4 \text{ MeV/nucleon}] .$$

It is important to recognize that $l_{\max}$ for this reaction is 340; hence, hundreds of l waves contribute to the cross section in this relatively narrow angular range. At this bombarding energy there is an indication that the laboratory differential cross section levels out for laboratory angles smaller than about 20°. This is interpreted to be due to an orbiting component in the reaction which is, however, less significant than observed for other Kr-induced reactions involving lighter targets, such as the ^{165}Ho + ^{84}Kr reaction.[5]

The center-of-mass angular distribution for light ($23 \leq Z \leq 46$) reaction products is given in Fig. 2 for final total kinetic energies in the range 240 MeV $\leq E \leq$ 480 MeV; i.e., very weakly and very strongly damped events are partially excluded. Note that the differential cross section is plotted on a logarithmic scale. The peak cross section is at $\theta_{\text{c.m.}} \approx 45°$, slightly forward of the center-of-mass quarter-point angle of $\theta_{1/4} \approx 50°$. The above angle of maximum reaction cross section is to be compared to 58° ($\theta_{1/4} \approx 66°$) and 95° for ^{84}Kr bombarding energies of 600 (Ref. 2) and 525 (Ref. 1) MeV, respectively. A similar shift in the angle of the peak cross section with bombarding energy to smaller angles has been reported for other very heavy reaction systems also, for example, ^{168}Er + ^{86}Kr (Ref. 18), ^{208}Pb + ^{84}Kr (Ref. 19), and ^{209}Bi + ^{136}Xe (Ref. 20).

The fragment Z (charge) distribution, shown in Fig. 3 only for the light Kr-like fragments, is essentially bimodal centered around the projectile Z and target Z. However, there is an asymmetry towards high Z values which could be taken as an indication of a small contribution by a second component which may be associated with a fusion-fission process with a symmetric charge distribution centered at $Z \approx 59$ and/or a sequential fission process with a symmetric charge distribution centered at a Z value of approximately 42. The reaction fragments included in Fig. 3 have final total kinetic energies in the range 240 MeV $\leq E \leq$ 480 MeV. Hence, very weakly damped events in the quasielastic region and very strongly damped events are excluded. As stat-

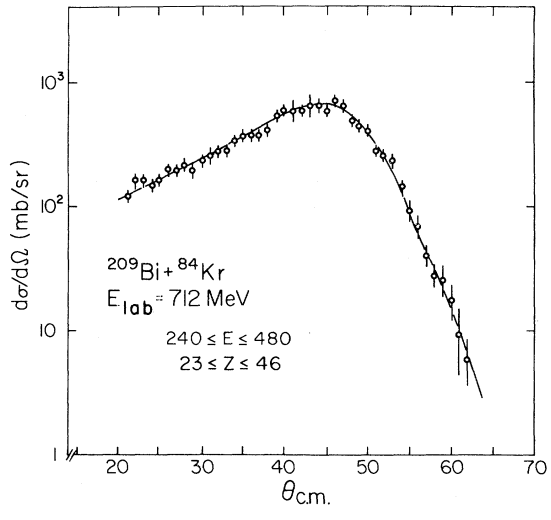

FIG. 2. Center-of-mass angular distribution for light reaction products with c.m. total kinetic energies E indicated.

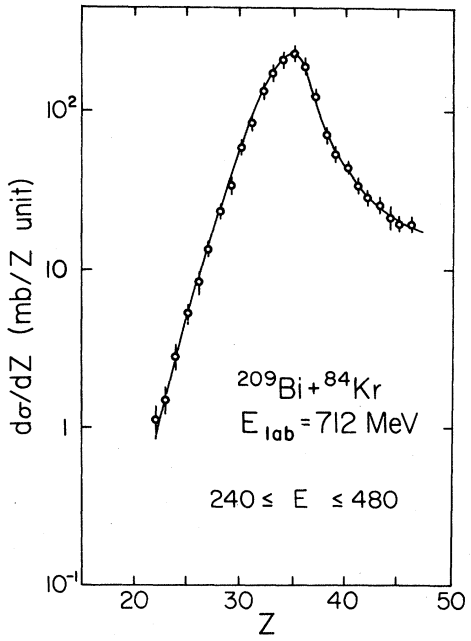

FIG. 3. Element (Z) distribution for the light (Kr-like) fragments.

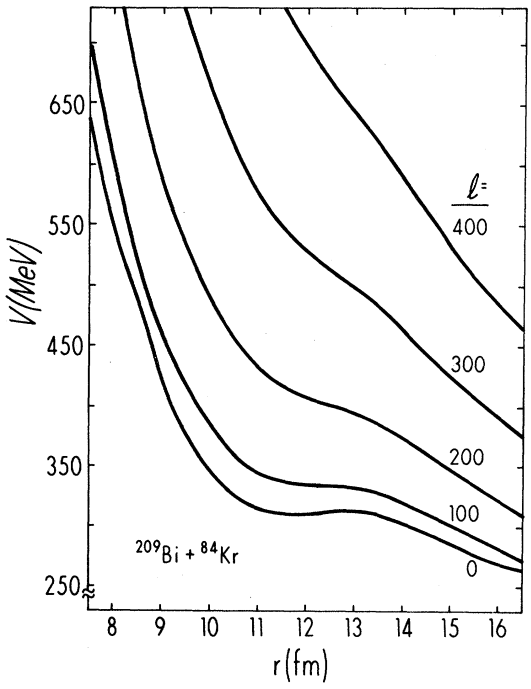

FIG. 4. Potential energy

$$V(r)=V_C(r)+V_l(r)+V_N(r)$$

as a function of separation distance r for five values of the angular momentum l. The nuclear proximity (Ref. 29) potential is used in the calculations.

ed previously, one possible explanation of asymmetry in the charge distribution shown in Fig. 3 requires a small contribution of a fusion-fission-like component. Such a component is known to exist for other heavy ion reactions[21–23] in this energy regime and there is some evidence that the magnitude of this component correlates with $(Z^2/A)_{\text{eff}}$,[24] where

$$(Z^2/A)_{\text{eff}}=4Z_PZ_T/A_P{}^{1/3}A_T{}^{1/3}(A_P{}^{1/3}+A_T{}^{1/3}),$$

a quantity first defined by Bass.[25] For the present reaction, the subtraction of a fusion-fission component, with a maximum cross section of 18 mb for fragments with symmetric Z and a width (FWHM) $\Gamma_Z=30$ units, from the charge distribution shown in Fig. 3 leaves a large residual contribution of damped reaction frgaments with a Z distribution which is approximately symmetrical around the projectile Z. The above values of width and cross section lead to a total fusion-fission-like reaction cross section of approximately 300 mb, a value in reasonable agreement with an upper limit of 240 mb established experimentally[5,26] and a calculation[22] based on a recent dynamical model of fusion.[27] In addition, for a value of $(Z^2/A)_{\text{eff}}=44.59$, a derived value of the ratio $(\sigma_{\text{CN}}+\sigma_{\text{FL}})/\sigma_R$ of 0.1 is in qualitative agreement with a systematic trend of this ratio for very heavy ion reactions.[24]

Sequential fission of the heavy Bi-like fragments[28] following the binary damped reaction process may contribute a cross section to the higher Z elements plotted in Fig. 3 also. This process would produce fragments having a maximum cross section in the vicinity of $Z\approx 43$ and a FWHM in Z of approximately 10 units. The present experiment did not differentiate sequential fission from fusion-fission and, hence, it is not possible to determine the relative contributions of these two processes to the data plotted in Fig. 3.

As indicated above, the dominant reaction component observed in a 712-MeV ^{84}Kr bombardment of ^{209}Bi is due to the damped or deep-inelastic reaction process, although small sequential fission and fusion-fission-like components may exist also. These results are consistent with expectations based on the relevant conservative potential energy V. In Fig. 4 the effective potential

$$V(r)=V_C(r)+V_l(r)+V_N(r)$$

is shown as a function of heavy-ion separation distance r for several values of the angular momentum l in units of $\hbar$. Here V_C, V_l, and V_N are the Coulomb, centrifugal, and nuclear proximity[29] interaction energies, respectively. Few, if any, l waves

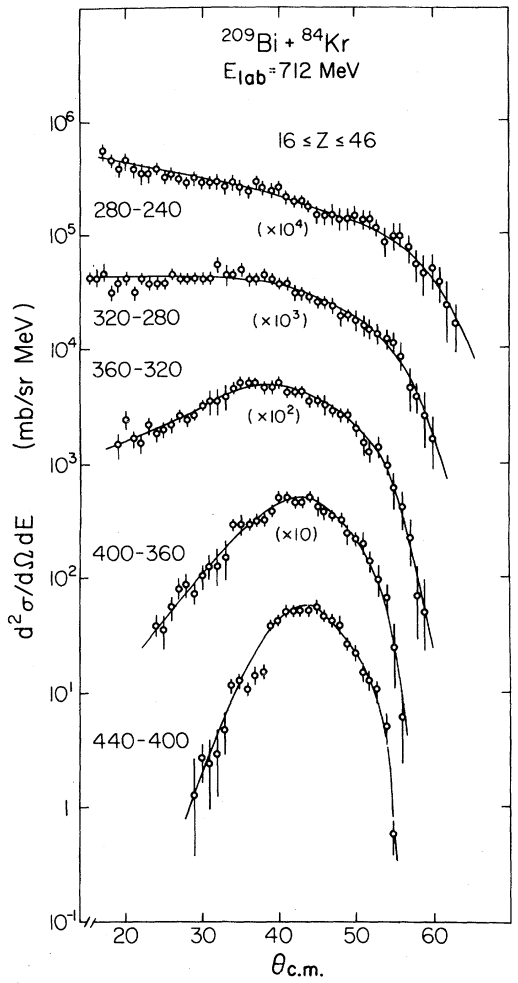

FIG. 5. Angular distribution of reaction products with $16 \leq Z \leq 46$ as a function of total kinetic energy E. Note that the energy bins are 40 MeV wide and that the highest energy bin containing quasielastic and weakly damped events is omitted. The scaling factor indicated under each curve has been used to multiply the experimental differential cross sections.

lead to pockets in the effective potential that could induce trapping of the system and, hence, yield long-lived composite nuclei. Even if the sudden-approximation or frozen density limit is relaxed for the nuclear proximity potential, the number of l waves corresponding to pockets in the effective potential based on the modified nuclear proximity potential remains rather small.

The fragment kinetic energy spectrum for the ^{209}Bi + ^{84}Kr reaction at $E_{\rm lab}=712$ MeV has been published previously.[3] There is a continuous range of total kinetic energy damping with a small peak in the differential cross section $d\sigma/dE$ in the quasielastic region and a very broad bump in the vicinity of the spherical Coulomb barrier. Final kinetic energies E range down to values more than 100 MeV below the energy associated with the Coulomb barrier for spherical fragments separated by the strong absorption radius $R_{\rm SA}$.

B. Correlations of experimental observables

In the previous section integral angular and charge distributions for all the reaction products from the ^{209}Bi + ^{84}Kr reaction are shown. For a more detailed study of the evolution of the damped reaction mechanism with interaction time or impact parameter, correlations of experimental variables with the amount of dissipated kinetic energy have proven very instructive.[17] As kinetic energy is dissipated in damped reactions, angular and Z distributions broaden drastically.

The angular distribution of the reaction products with $16 \leq Z \leq 46$ are shown in Fig. 5 as a function of the final kinetic energy E, where the energy bins are 40 MeV wide. The angular distribution for the most weakly damped quasielastic energy bin is omitted from this figure. The angular distributions show a smooth progression from sideways peaking to forward peaking with decreasing final total kinetic energy E.

Angular distributions for reaction fragments of particular Z, where the bin size is 3 units, are shown in Fig. 6. In the vicinity of the projectile Z, the angular distribution is sideways peaked. As Z is increased or decreased, the angular distribution becomes more forward peaked. However, the forward peaking sets in for smaller absolute values of the quantity $|Z-36|$ when $Z>36$ than when $Z<36$. This appears to be evidence for some asymmetry in the interaction times for projectilelike fragments of charges $Z_P+\Delta Z$ and $Z_P-\Delta Z$.

In contrast to Fig. 5 where the angular distributions of fragments with $16 \leq Z \leq 46$ are shown as a function of total kinetic energy, the angular distributions shown in Fig. 7 are for a Z bin, $35 \leq Z \leq 37$, centered at Z_P. The energy bins in Fig. 7 are 80 MeV wide. From a comparison of the shapes of the angular distributions in Figs. 5 and 7, one concludes that the shape of the angular distribution depends on the final kinetic energy but is independent of Z. This illustrates the primary role of the energy loss as a determinant of the damped reaction features, rather than one of the reaction angle or Z value. Because of the marked change of the angular distributions with reaction-product charge Z (see Fig. 6),

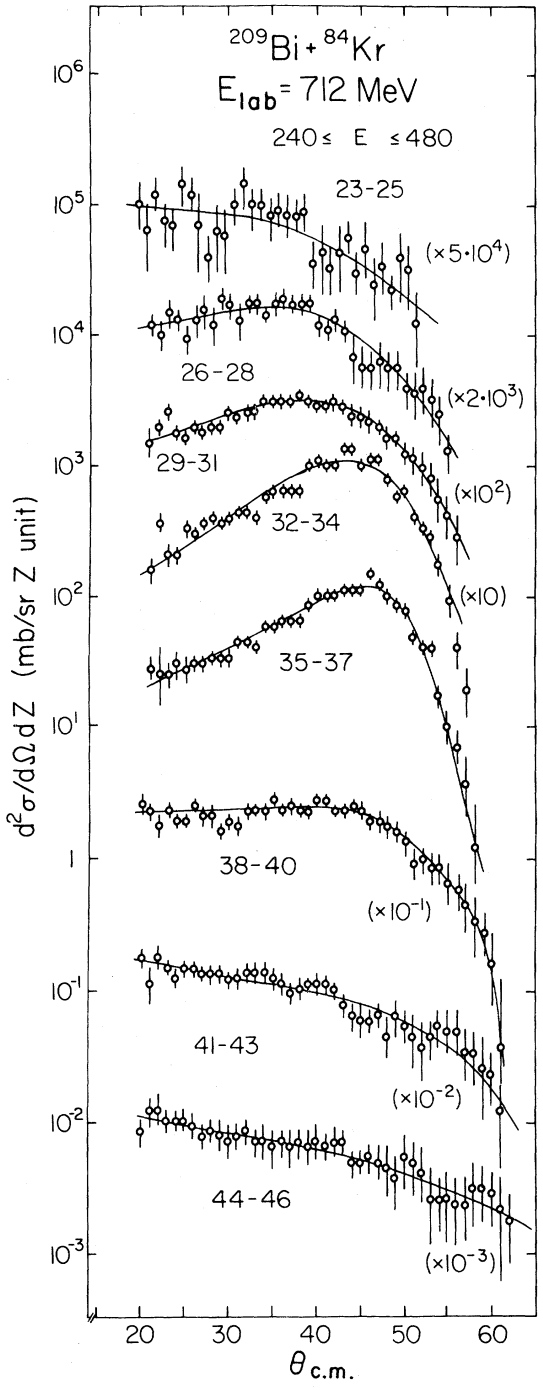

FIG. 6. Angular distributions for reaction fragments in a given Z bin. Bin size is 3 units of Z. See caption of Fig. 5 for the definition of scaling factors on right of figure.

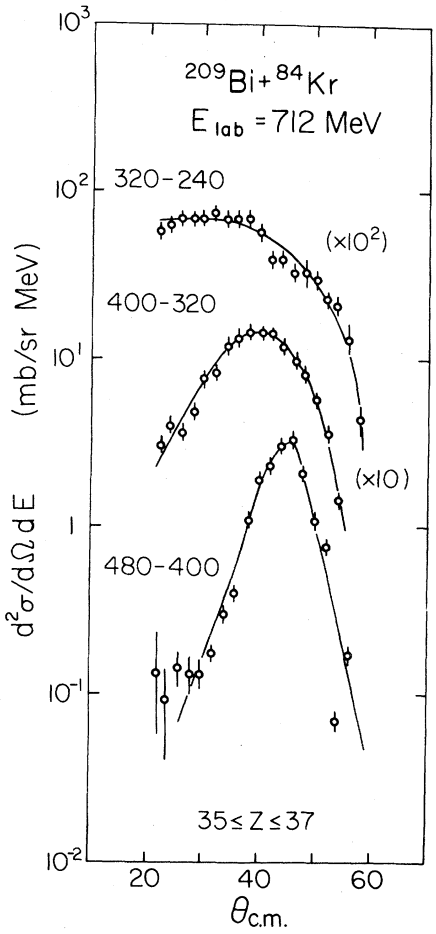

FIG. 7. Differential cross section for fragments near the projectile ($35 \leq Z \leq 37$) as a function of total kinetic energy for three 80-MeV wide energy bins. See caption of Fig. 5 for the definition of scaling factors on right of figure.

the assumption has been made that the net charge transfer is a measure of the lifetime of the intermediate dinuclear system. That is, elements near the projectile, which display strong side peaking, arise from short interaction times, whereas elements far from the projectile, which show broadened angular distributions, arise from long interaction times. However, this correlation is not a primary one. It is true that the elements near the projectile are dominant in the angular distributions with strong side peaking where the interaction times are short. It is true also that elements far from the projectile are associated mainly with broad or forward-peaked angular distributions where the interaction times are long. These secondary correlations arise through common correlations with energy loss. It is equally true, as shown in Fig. 7, that elements near the projectile with large energy losses have angular distributions similar to those of elements far from the projectile in the same kinetic energy bin (see Fig. 5).

The double differential cross section $d^2\sigma/dE\, dZ$

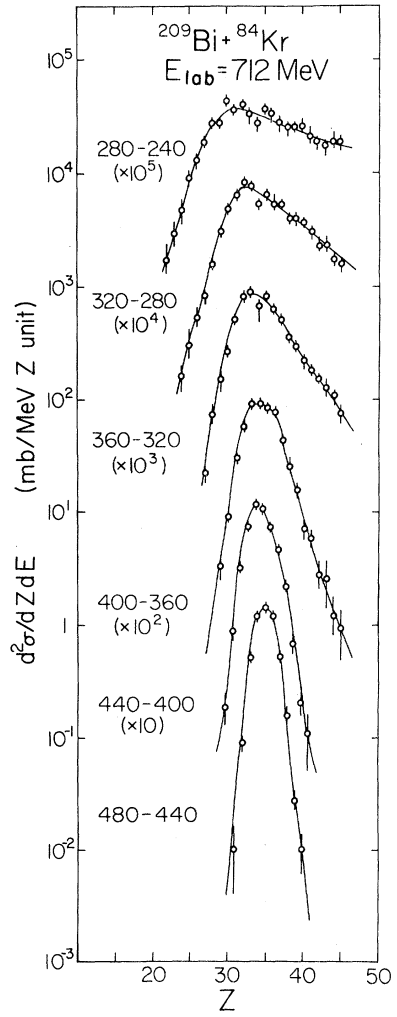

FIG. 8. Charge (Z) distribution as a function of total kinetic energy for energy bins 40 MeV wide. See caption of Fig. 5 for the definition of the scaling factors listed under each energy bin.

for the ^{209}Bi + ^{84}Kr reaction is plotted as a function of reaction product Z in Fig. 8. For the highest kinetic energies, the Z distributions plotted in Fig. 8 are Gaussian in shape. The quasielastic events with center-of-mass kinetic energies between 480 and 507 MeV are not included in this figure. As the kinetic energy decreases (i.e., with increasing kinetic energy dissipation), the Z distributions widen, as first reported[3,30] for Kr- and Xe-induced reactions on heavy targets, a phenomenon now known to be a characteristic property of heavy ion reactions. For the present reaction at the smaller kinetic energies, the Z distributions become slightly skewed. This may be due to a contribution from a second reaction mechanism (the fusion-fission process) where the Z distribution is broad and essentially symmetric around $Z \approx (Z_P + Z_T)/2$. It has been postulated that such a component may underlie the Z distributions reported for other heavy ion damped reactions.[24] The verification of this postulate, however, must await the results of more detailed and systematic experimental studies.

Heavy-ion reactions at relatively low bombarding energies, such as that studied here, are expected to be influenced by the appropriate multidimensional potential energy surface. Figure 9 shows the contour lines of potential energy surfaces of the dinuclear complex consisting of two spherical nuclei as calculated from the liquid-drop model including shell corrections. The energy contours are plotted versus neutron number N_1 and atomic number Z_1 for the light (Kr-like) fragments. The potential contains the sum of the fragment binding energies, the Coulomb, nuclear, and centrifugal potentials, and has the form

$$V(Z_1,N_1) = V_{\rm LD}(Z_1,N_1) + V_{\rm LD}(Z_2,N_2) + V_{\rm Coul}(Z_1,Z_2,r) + V_{\rm nucl}(A_1,A_2,r,\rho) + \frac{\hbar^2 l^2}{2\mu r^2} - U_0 \, .$$

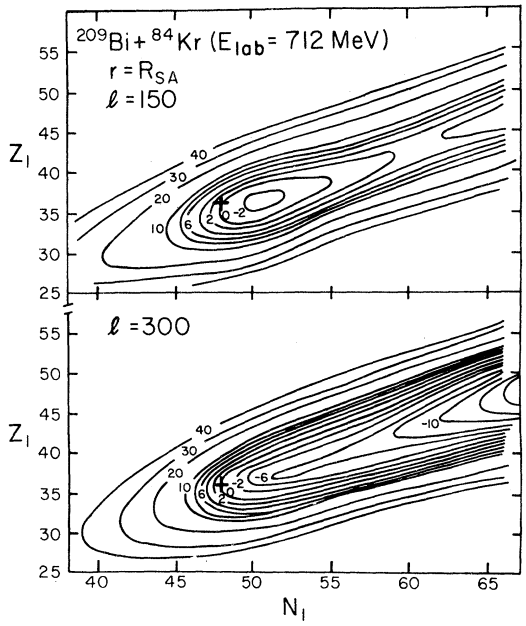

FIG. 9. Potential energy surfaces calculated from the liquid drop model (with shell corrections) for the dinuclear complex; (a) $l = 150\hbar$, (b) $= 300\hbar$. The cross signifies the injection point.

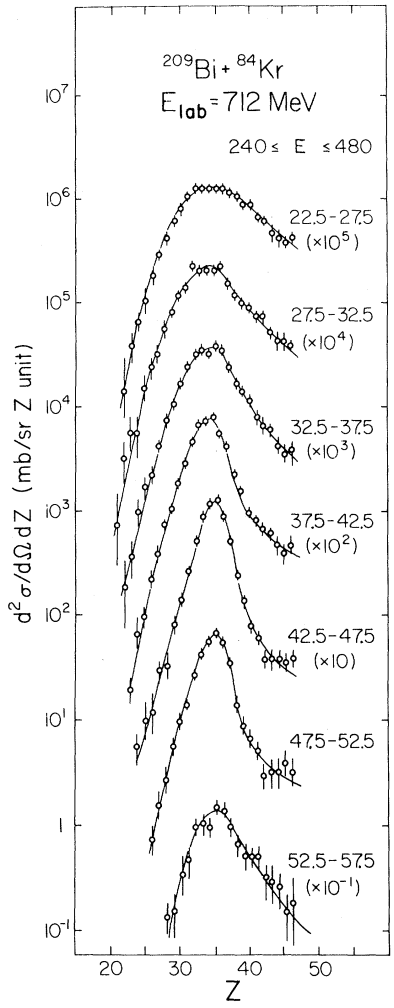

FIG. 10. Double differential cross section as a function of element (Z) for angular bins 5° wide. Under each range of angles is the cross section scaling factor defined in the caption of Fig. 5.

In the above equation, the constant U_0 is chosen so that the initial fragmentation (denoted by a cross in the figure) is normalized to zero at a separation distance equal to the strong-absorption radius R_{SA}.

The energy contours in Fig. 9 are constructed for $l=150\hbar$ and $300\hbar$, respectively. Although such simple surfaces are somewhat unrealistic, one might predict, on the basis of the static potentials alone, some average drift of the mass and charge distributions towards symmetry. The experimental drift in the first moment of the Z distribution, however, seems to be slightly in the opposite direction to smaller values of $\langle Z \rangle$. It is conceivable that the particular shape of the fragment Z distribution is distorted due to undetected secondary evaporation processes. However, the extent to which the emission of light charged particles influences $\langle Z \rangle$ is unknown at present for Kr-induced reactions.

The element distributions for fixed angular ranges are plotted in Fig. 10. Here the double differential cross section $d^2\sigma/d\Omega\, dZ$ is plotted as a function of atomic number Z for a given angular range of 5°. As one moves away from the angle of 45° where the cross section is a maximum (see Fig. 2), the distributions widen and become somewhat more skewed. This is expected since the relative yield of events with higher kinetic energy losses increases for these angles.

Variances $\sigma_Z{}^2$ of the Z distributions of the light (Kr-like) fragments shown in Fig. 8 are plotted as a function of kinetic energy loss $(-Q)$ in Fig. 11, where $E_{\rm loss}=-Q=E_{\rm c.m.}-E$. The variances shown in Fig. 11 for the two higher kinetic energy loss values have been deduced primarily from the lower-Z data. Substantial errors are assigned to these data points due to the non-Gaussian shapes of the experimental element Z distributions.

IV. MICROSCOPIC INTERPRETATION OF DATA

A. Simple nontrajectory model

In a phenomenological model described earlier,[3,17,31,32] use was made of the microscopic time scale provided by the nucleon-exchange mechanism to derive a dissipation rate

$$-\frac{dT}{dN_{\rm ex}}=\alpha(m/\mu)T \tag{1}$$

with respect to the number of nucleons exchanged $N_{\rm ex}$, where $N_{\rm ex}$ was related to the measured variances, $\sigma_Z{}^2$ or $\sigma_A{}^2$. In Eq. (1),

$$T=E_{\rm c.m.}-V_{\rm Coul}-E_{\rm loss}$$

is the available relative kinetic energy above the Coulomb barrier $V_{\rm Coul}$, m is the nucleon mass, and μ is the reduced mass of the dinuclear system. The coefficient α conveys information on the character of the dissipation mechanism. Equation (1) implies that the recoil momentum due to a nucleon exchange is completely dissipated before a subsequent process occurs.

The experimental dependence of α on bombarding energy has been interpreted[33] in terms of Pauli blocking. Based on a model developed by Randrup,[34,35] it has been shown[33] that

$$\alpha=(T_F/2\tau^*)[\Psi(\zeta)/X(\zeta)]\ ,$$

where T_F is the Fermi energy and

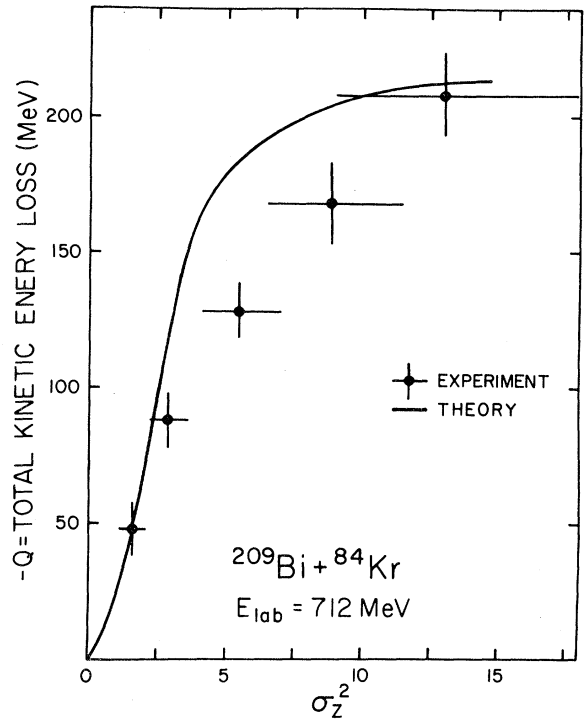

FIG. 11. Experimental variances σ_Z^2 plotted as a function of the total kinetic loss $(-Q)$. The solid line is calculated with the reaction model described in Sec. IV B.

$$\tau^* = \langle \tfrac{1}{2}\omega \coth(\omega/2\tau) \rangle_F$$

is an "effective temperature" giving a measure of the energy interval around the Fermi level contributing to the exchange processes. The expression in the bracket represents the ratio of the dimensionless form factors[34] for the friction coefficient (Ψ) and the mass transport coefficient (X). The parameter ζ represents the surface separation s in units of b (≈ 1 fm). The quantity $\omega = F_A - \vec{U}\cdot\vec{p}$ is the amount of intrinsic excitation produced by an exchange of a nucleon with intrinsic momentum $\vec{p}$, and the brackets denote an average over the orbitals in the Fermi surface. The energy dissipation is assumed to be due to the exchange of nucleons between two Fermi-Dirac gases in slow relative motion characterized by the relative velocity $\vec{U}$. The two gases have a common temperature τ, and their Fermi energies ϵ_F differ by an amount F_A which is the static driving force for the mass-asymmetry degree of freedom represented by the mass number A of the projectilelike fragment.

Application of the Randrup model,[33,24] as outlined above for systems with $F_A \approx 0$ and peripheral collisions, leads to following version of Eq. (1)

$$-\frac{dT}{dN_{ex}} \approx -\left[\frac{\sigma_Z^2}{\sigma_N^2+\sigma_Z^2}\right]_T \frac{dT}{d\sigma_Z^2} \approx \frac{3\pi}{8}\left[\frac{m}{\mu}T_F T\right]^{1/2}\left[\frac{\Psi(\zeta)}{X(\zeta)}\right], \quad (2)$$

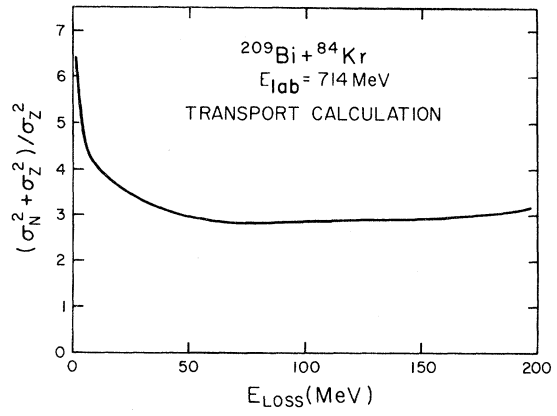

FIG. 12. Model calculations of $(\sigma_N^2+\sigma_Z^2)/\sigma_Z^2$ as described on Sec. IV B.

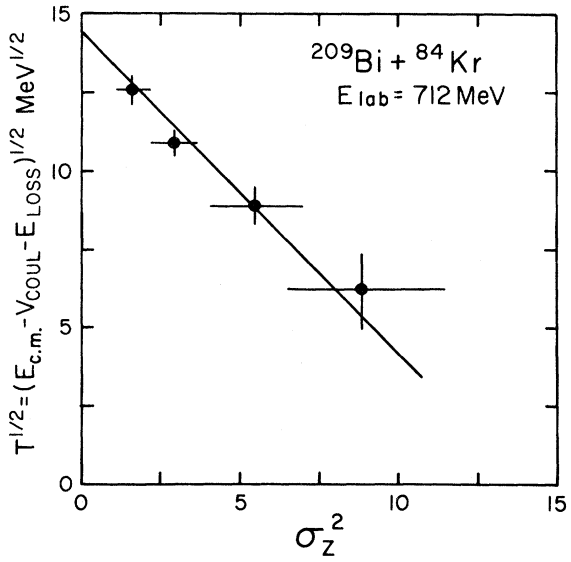

FIG. 13. Correlation of the available kinetic energy T with σ_Z^2. The solid line represents a simple model calculation [Eq. (3)] with

$$(\sigma_N^2+\sigma_Z^2)/\sigma_Z^2 = 3.0$$

and

$$\langle \Psi(\zeta)/X(\zeta) \rangle = 0.73 .$$

where $-dT/dN_{ex}$ is approximated by the product

$$-[\sigma_Z{}^2/(\sigma_N{}^2+\sigma_Z{}^2)]_T(dT/d\sigma_Z{}^2) .$$

Experimental charge and mass distribution data for heavy-ion dissipative collisions relate the final kinetic energy E (or the available energy T or the total kinetic energy loss E_{loss}) with a variance ($\sigma_Z{}^2$ or $\sigma_A{}^2$). Hence, the theoretical quantities of primary interest for comparison with experiment are those resulting from an integration over the total trajectory. However, it is not possible to integrate Eq. (2) without making simplifying assumptions about the quantities $[(\sigma_N{}^2+\sigma_Z{}^2)/\sigma_Z{}^2]_T$ and $[\Psi(\xi)/X(\xi)]$. Model calculations (see Sec. IV B) have shown that $[(\sigma_N{}^2+\sigma_Z{}^2)/\sigma_Z{}^2]_T$ is nearly constant with E_{loss} (or T), except for small total kinetic energy losses as shown in Fig. 12. Similar model calculations show, however, that the form factor ratio $[\Psi(\xi)/X(\xi)]$ increases with energy loss. Equation (2) has been integrated ignoring the energy dependence of the above two quantities to give

$$T^{1/2}=T_0^{1/2}-\frac{3\pi}{16}\left[\frac{m}{\mu}T_F\right]^{1/2}\left[\frac{\sigma_N{}^2+\sigma_Z{}^2}{\sigma_Z{}^2}\right]\left\langle\frac{\Psi(\xi)}{X(\xi)}\right\rangle\sigma_Z{}^2 . \tag{3}$$

The square root of the available energy

$$T=E_{c.m.}-V_{Coul}-E_{loss}$$

for the ^{209}Bi + ^{84}Kr reaction at a laboratory energy of 712 MeV is plotted in Fig. 13 as a function of the Z variance, $\sigma_Z{}^2$. In the evaluation of T the Coulomb barrier $V_{Coul}=301$ MeV was evaluated at the strong absorption radius R_{SA}. In the limit where $\sigma_Z{}^2=0$, the abscissa is given by $T_0^{1/2}=14.4$ MeV$^{1/2}$. The slope of the solid line is calculated [see Eq. (3)] with the assumptions that

$$(\sigma_N{}^2+\sigma_Z{}^2)/\sigma_Z{}^2=3.0$$

(see Fig. 12) and

$$\langle\Psi(\xi)/X(\xi)\rangle=0.73 ,$$

and furthermore that both quantities are energy independent. Although a reasonable fit to the data is obtained with Eq. (3), this agreement may be somewhat fortuitous since Eq. (3) is valid only for peripheral collisions of symmetric nuclei where both F_A and the component U_n of the relative velocity normal to the interface between the reaction partners can be neglected, conditions which are not fulfilled for the present data. In addition, the form factor ratio is changing with energy and its average value,

$$\langle\Psi(\xi)/X(\xi)\rangle=0.73 ,$$

has been adjusted here for a best fit to the data. The ^{209}Bi + ^{136}Xe data at three bombarding energies have been fitted with Eq. (3) also[24] and simplified versions of Eq. (3) have been applied by others.[36,37]

This simple theory, as exemplified by the solid line in Fig. 13, predicts a limiting value of $\sigma_Z{}^2$ of 14.2 when $T=0$. Experimentally, some values of the variance $\sigma_Z{}^2$ exceed this limit. These larger variances are associated with exit channels where the dinuclear complex is deformed prior to scission and the total kinetic energy loss is larger than

$$T_0=E_{c.m.}-V_{Coul} .$$

B. Trajectory model

In this section some of the data from the ^{209}Bi + ^{84}Kr reaction will be compared to a recent dynamical reaction model.[34,35] However, before making this comparison, a brief description of the model will be given. This one-body transport model is based on a small number of fundamental postulates and yields predictions for a wide range of reaction phenomena. The model assumes that average values of macroscopic variables specifying the relative motion, angular momentum, mass, charge, and mass-to-charge symmetry follow classical Lagrange-Rayleigh equations of motion. Statistical fluctuations of these coordinates are induced by the exchange of individual nucleons between the interacting nuclei described in terms of Fermi-Dirac gases at thermal equilibrium.

Adopting a relatively simple family of nuclear shapes featuring a neck between two spherical fragments, as illustrated in Fig. 14, the reaction dynamics of a dinuclear system is described by a set of macroscopic coordinates

$$\{\vec{q},\dot{\vec{q}}\}=\{r,\theta,\theta_P,\theta_T,\rho,A_L,Z_L,\tau,\Delta\tau,\dot{r},\dot{\theta},\dot{\theta}_p,\ldots,\} \tag{4}$$

some of which are defined in Fig. 14. The quantities A_L and Z_L are the mass and charge, respectively, of the light spherical fragment, τ is the average temperature of the system, and $\Delta\tau$ is the difference of the temperatures of light and heavy fragments. The time evolution of this set of average coordinates is assumed to follow from the Lagrange-Rayleigh equation of motion

$$\left\{\frac{d}{dt}\frac{\partial}{\partial\dot{\bar{q}}_i}-\frac{\partial}{\partial\bar{q}_i}\right\}\mathscr{L}=-\frac{\partial}{\partial\dot{\bar{q}}_i}\mathscr{F}\ . \tag{5}$$

Here, $\mathscr{L}=T-V$ is the Lagrangian, and $\mathscr{F}$ is the dissipation function. In a transport approach, a two-dimensional Fokker-Planck equation[38,39]

$$\frac{\partial}{\partial t}P=\left[-\frac{\partial}{\partial N}V_N-\frac{\partial}{\partial Z}V_Z+\frac{\partial^2}{\partial N^2}D_{NN}+\frac{\partial^2}{\partial Z^2}D_{ZZ}+2\frac{\partial^2}{\partial N\partial Z}D_{NZ}\right]P \tag{6}$$

is expected to govern the dynamical evolution of the probability $P(N,Z,t)$ for finding N neutrons and Z protons in the projectilelike reaction partner. The physical information on the microscopic transition probabilities at each time t is contained in the appropriate transport coefficients. Average neutron and proton numbers are predicted to change with rates determined only by the drift coefficients, according to $\partial\bar{N}/\partial t\approx V_N$ and $\partial\bar{Z}/\partial t\approx V_Z$, whereas the growth of the corresponding covariances of the probability distribution depends on diffusion and drift coefficients, as well as on the covariances already accumulated.[40] Evaluated along the mean trajectory $[\bar{N}(t),\bar{Z}(t)]$, these growth rates can be written as

$$\begin{aligned}
\frac{\partial\sigma_N{}^2}{\partial t}&\approx 2\left[D_{NN}+\sigma_N{}^2\frac{\partial V_N}{\partial N}+\sigma_{NZ}\frac{\partial V_N}{\partial Z}\right],\\
\frac{\partial\sigma_Z{}^2}{\partial t}&\approx 2\left[D_{ZZ}+\sigma_Z{}^2\frac{\partial V_Z}{\partial Z}+\sigma_{NZ}\frac{\partial V_Z}{\partial N}\right],\\
\frac{\partial\sigma_{NZ}}{\partial t}&\approx 2D_{NZ}+\sigma_N{}^2\frac{\partial V_Z}{\partial N}+\sigma_Z{}^2\frac{\partial V_N}{\partial Z}+\sigma_{NZ}\left[\frac{\partial V_N}{\partial N}+\frac{\partial V_Z}{\partial Z}\right].
\end{aligned} \tag{7}$$

The dispersion $\sigma_A{}^2$ of the mass number $A=N+Z$ of the projectilelike fragment can subsequently be obtained from the relation

$$\sigma_A{}^2=\sigma_N{}^2+\sigma_Z{}^2+2\sigma_{NZ}\ .$$

In the derivation of Eq. (7) from the Fokker-Planck equation, an account is given of the confinements imposed on the transport processes by the variation of the drift coefficients with N and Z. These constraints, mainly due to curvature and alignment of the underlying time-dependent potential energy surface, are more restrictive for larger variances and enforce the proper equilibrium variances. Although the mixed diffusion coefficient D_{NZ} vanishes in the model, owing to the statistical independence of individual exchanges, a covariance σ_{NZ} develops nevertheless with time, according to Eq. (7), because the underlying potential energy surface is misaligned with respect to the N-Z coordinate system (see Fig. 9).

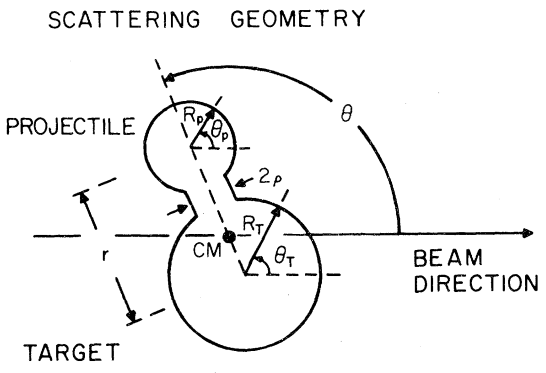

FIG. 14. Scattering geometry for dynamical reaction model (see Sec. IV B).

The total interaction potential (see Fig. 9) contains the sum of the fragment binding energies calculated from the liquid drop model including shell corrections, and the Coulomb, nuclear, and centrifugal potentials. The nuclear potential is given by[41]

$$V_{\rm nucl}(\rho,s)=2\pi\gamma\rho d_{\rm eff}-2\pi\gamma\rho^2+4\pi\gamma\bar{R}b\Phi(d/b)\exp\{-\rho^2/2\bar{R}b\}\ . \tag{8}$$

The various quantities have the usual notation of the proximity theory.[29,42] The first term in Eq. (8) gives the liquid-drop energy of the cylindrical neck surface produced, where $d_{\rm eff}$ is the effective length of the neck and ρ its radius. The second term describes the energy of the spherical caps dissolved, and the last term is the proximity energy of the opposing surfaces outside the neck region, modified by an exponential factor due to their inclination with respect to each other. The effective length $d_{\rm eff}$ is somewhat smaller than its apparent length

$$d \approx s + \rho^2/2\bar{R} ,$$

because the proximity interaction already accounts for the creation of a minimum neck when two parallel surfaces are at a distance of $s_{\rm cr} \approx 1.8$ fm. The proximity correction is assumed to vanish with large neck radii as $s_{\rm cr}(1-\rho/2\bar{R})$ owing to an increasing relative inclination of opposing surface elements. The potential of Eq. (8) is shallower than both the standard and modified proximity potentials for intermediate separation distances but approaches them closely in the tail region around the strong-absorption radius $R_{\rm SA}$ where the latter are quite well established by elastic-scattering studies.

The dissipation function of Eq. (5) contains terms arising from the relative motion, the neck motion, and changes in the average mass and charge asymmetries. The friction force acting on the relative motion is assumed to be mainly due to the recoil induced by nucleons passing through a transparent window between the collision partners as described by the "window formula."[41] This term is usually given by

$$\mathcal{F}_{\rm ex} = -\tfrac{1}{2}\frac{dT}{dt} \approx \langle \omega^2 \rangle_F (n_0/m)(2\pi\bar{R}b/T_F)\Psi(\zeta) , \tag{9}$$

where (n_0/m) is the one-way bulk flux in standard nuclear matter and equal to 2.55×10^{21} nucleons $\sec^{-1}\,\mathrm{fm}^{-2}$ and all the other quantities have been defined previously. The transmission function $\Psi(\zeta)$ appearing in Eq. (9) is replaced by the form

$$\bar{\Psi}(\rho,s) = (\rho^2/2\bar{R}b) + \Psi(d/b)\exp(-\rho^2/2\bar{R}b) \tag{10}$$

in a manner consistent with the form of Eq. (8) adopted for the interaction potential. In the above equation Ψ is the ordinary proximity flux function describing the transparency to nucleon exchange of two juxtaposed nuclear surfaces. The dissipation function contains also a term

$$\mathcal{F}_{\rm drift} = \tfrac{1}{2}(F_Z V_Z + F_N V_N)$$

which accounts for the change in binding energies induced by the exchange of nucleons, which is, however, usually relatively small. The damping of the neck motion arises from collisions of nucleons with its walls (wall formula).[41] This motion is assumed to be overdamped and the corresponding dissipation function is given by

$$\mathcal{F}_{\rm neck} = \{4\pi n_0 \rho d \exp[-d/(\rho+b)]\}\dot{\rho}^2 . \tag{11}$$

In the Randrup model,[34,35] transport of mass, charge, energy, linear, and angular momentum in a damped reaction is attributed to the stochastic exchange of individual nucleons between reaction partners, taking proper account of the Pauli exclusion principle. The model transport coefficients have the form

$$\begin{aligned} &V_N = N_N' F_N, \quad V_Z = N_Z' F_Z , \\ &D_{NN} = N_N' \tau_N^*, \quad D_{ZZ} = N_Z' \tau_Z^*, \quad D_{NZ} = 0 , \end{aligned} \tag{12}$$

where the differential current of neutrons (N_N') or protons (N_Z') exchanged between the Fermi-Dirac gases is calculated without accounting for the Pauli blocking effect. The various quantities needed to calculate the transport coefficients are defined by Randrup. Whereas in a classical diffusion model, the diffusion coefficient is proportional to the nuclear temperature τ, a quantum-statistical approach has to account for Pauli blocking which excludes from participation in the diffusion process those single-particle orbits that correspond to the overlap of the Fermi momentum spheres of the two interacting nuclei. This overlap is dependent both on the temperature and the relative velocity. The behavior of τ and τ^* with energy loss is illustrated for the $^{209}\mathrm{Bi} + {}^{136}\mathrm{Xe}$ reaction elsewhere.[43] Early in the reaction, where there is comparatively little overlap of the two Fermi momentum spheres, which are displaced because of the relative velocity, the Pauli blocking is less effective and relatively many levels are available for nucleon exchange, resulting in large values of τ^*. At higher energy losses, where the relative velocity is small, Pauli blocking is more effective and τ^* decreases, eventually approaching the nuclear temperature τ.

In the above microscopic theory, the nuclear potential $V_{\rm nucl}$,[29,42] the dissipation function $\mathcal{F}$ (Refs. 44 and 45), and the transport coefficients[34,35] are calculated in a consistent way. The present calculations have been performed with the Bondorf-Coulomb potential.[46,47] Hence, there are no remain-

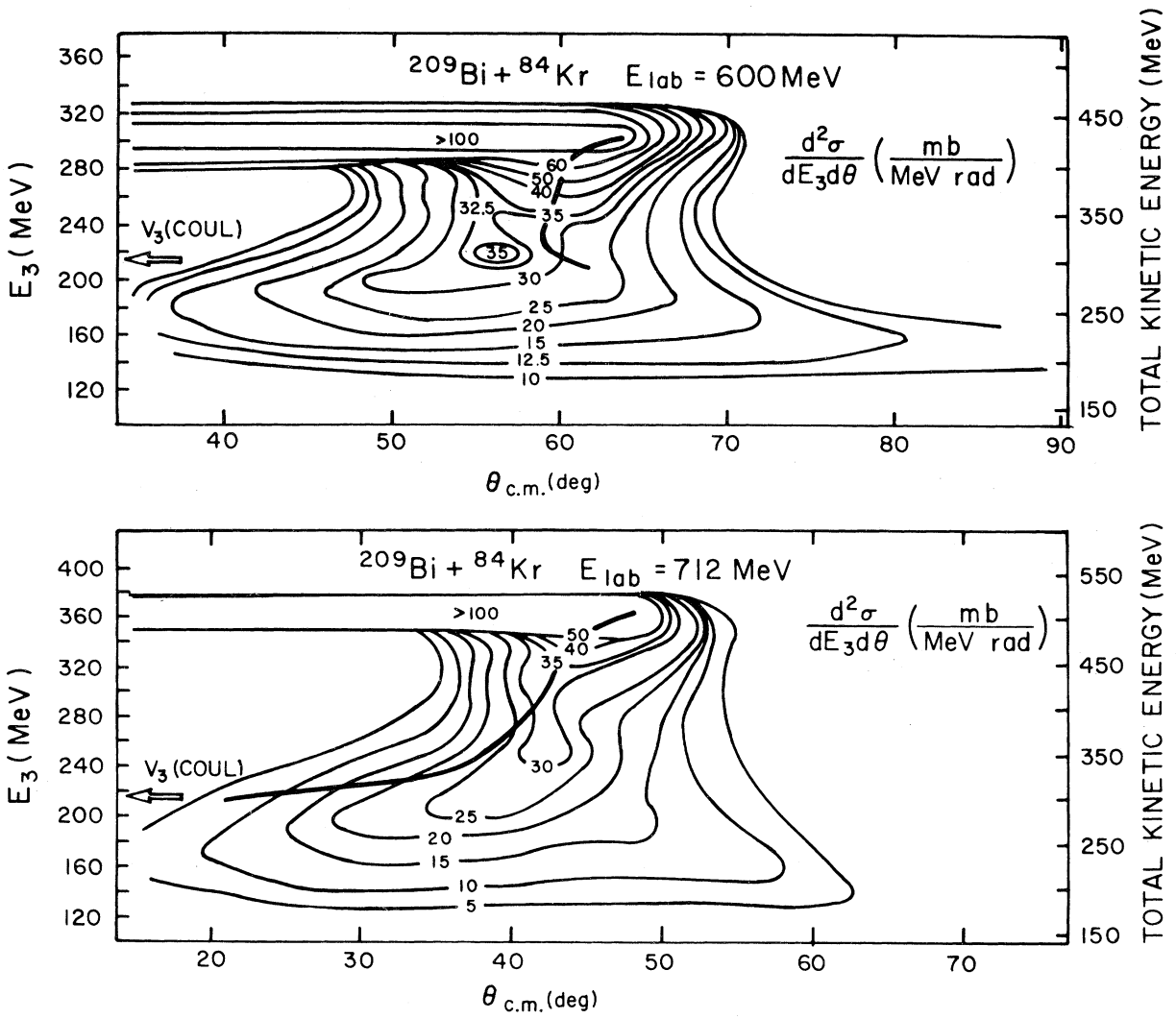

FIG. 15. Constant contours of $d^2\sigma/dE_3d\theta$ as a function of the center-of-mass energy E_3 of the light (Kr-like) fragment and the center-of-mass angle $\theta_{c.m.}$. These contours were generated in an event-by-event analysis of singles energy spectra assuming the mass of the detected product was 84. The ridge labeled >100 corresponds in each case to elastic scattering. Multiplication of E_3 and V_3 (Coul) by the factor (293/209) converts these energies to the total kinetic energy E (scale on right) and the Coulomb energy V_{Coul}, respectively.

ing adjustable parameters in the calculation. Employing this theoretical model, the correlation between the total kinetic energy loss $(-Q)$ and the variance $\sigma_Z{}^2$ has been calculated for the ^{209}Bi + ^{84}Kr reaction and is shown in Fig. 11. As can be seen in this figure, qualitative agreement between the theory including correlated nucleon exchange and experiment is obtained. It is noteworthy that the calculation predicts a small (0.3 – 1.0 Z unit) negative drift of the centroid of the charge distribution for the highest energy losses which is also in qualitative agreement with the evolution of the peak in the experimental distributions (cf. Fig. 8).

In Fig. 15 the theoretical total kinetic energy and scattering angle for a series of impact parameters are compared with the experimental Wilczyński plots for the ^{209}Bi + ^{84}Kr reaction at laboratory bombarding energies of 600 and 712 MeV. The theory reproduced qualitatively the overall average behavior of the experimental data. The general quality of agreement between the present theory and experiment is equivalent to that obtained with time-dependent Hartree-Fock calculations.[13]

ACKNOWLEDGMENTS

This work was supported by the U.S. Department of Energy. The use of the facilities at the Nuclear Structure Research Laboratory was supported by the National Science Foundation. The authors would like to acknowledge the hospitality extended to them at the Lawrence Berkeley Laboratory and thank H. Grunder and the staff of the SuperHILAC for providing an efficient operation of the accelerator.

---

*Present address: Ruhr-Universität Bochum, 4630 Bochum, West Germany.

†Present address: Chemistry Department, Indiana University, Bloomington, IN 47405.

[1]F. Hanappe, M. Lefort, C. Ngô, J. Péter, and B. Tamain, Phys. Rev. Lett. 32, 738 (1974).

[2]K. L. Wolf, J. P. Unik, J. R. Huizenga, J. R. Birkelund, H. Freiesleben, and V. E. Viola, Phys. Rev. Lett. 33, 1105 (1974).

[3]J. R. Huizenga, J. R. Birkelund, W. U. Schröder, K. L. Wolf, and V. E. Viola, Jr., Phys. Rev. Lett. 37, 885 (1976).

[4]J. R. Huizenga, 169th American Chemical Society Meeting in Philadelphia, Pennsylvania, 1975.

[5]K. L. Wolf and C. T. Roche, Proceedings of the Symposium on Macroscopic Features of Heavy Ion Collisions, Argonne National Laboratory Report ANL/PHY-76-2, 1976, Vol. I, p. 295.

[6]W. U. Schröder, J. R. Birkelund, J. R. Huizenga, K. L. Wolf, J. P. Unik, and V. E. Viola, Jr., Proceedings of the European Conference on Nuclear Physics with Heavy Ions, Caen, France, 1976, p. 178.

[7]J. P. Bondorf, J. R. Huizenga, M. I. Sobel, and D. Sperber, Phys. Rev. C 11, 1265 (1975).

[8]M. G. Mustafa, Phys. Rev. C 14, 2168 (1976).

[9]L. Lin, A. Sherman, and D. Sperber, Phys. Rev. Lett. 37, 327 (1976).

[10]J. N. De and D. Sperber, Phys. Lett. 72B, 293 (1978).

[11]A. Sherman, D. Sperber, M. I. Sobel, and J. P. Bondorf, Z. Phys. A 286, 11 (1978).

[12]S. K. Samaddar, M. I. Sobel, J. N. De, S. I. A. Garpman, D. Sperber, M. Zielinska-Pfabe, and S. Moller, Nucl. Phys. A332, 210 (1979).

[13]K. T. R. Davies and S. E. Koonin, Phys. Rev. C 23, 2042 (1981).

[14]G. J. Ball and S. E. Koonin, California Institute of Technology Report MAP 24, 1982.

[15]J. R. Birkelund, J. R. Huizenga, H. Freiesleben, K. L. Wolf, J. P. Unik, and V. E. Viola, Jr., Phys. Rev. C 13, 133 (1976).

[16]Jiang Cheng-Lie, P. R. Christensen, Ole Hansen, S. Pontoppidan, F. Videbaek, D. Schüll, Shen Wen-Qing, A. J. Baltz, P. D. Bond, H. Freiesleben, F. Busch, and E. R. Flynn, Phys. Rev. Lett. 47, 1039 (1981).

[17]W. U. Schröder and J. R. Huizenga, Annu. Rev. Nucl. Sci. 27, 465 (1977).

[18]A. Gobbi and W. Nörenberg, *Heavy Ion Collision,* edited by R. Bock (North-Holland, Amsterdam, 1980), p. 128.

[19]R. Vandenbosch, M. P. Webb, and T. D. Thomas, Phys. Rev. Lett. 36, 459 (1976).

[20]J. R. Huizenga, J. R. Birkelund, W. U. Schröder, W. W. Wilcke, and H. J. Wollersheim *Proceedings of the Nuclear Physics Workshop, Trieste, Italy,* edited by C. H. Dasso (North-Holland, Amsterdam, 1981), p. 583.

[21]H. Sann, R. Bock, Y. T. Chu, A. Gobbi, A. Olmi, U. Lynen, W. Müller, S. Bjørnholm, and E. Esbensen, Phys. Rev. Lett. 47, 1248 (1981).

[22]J. R. Huizenga, J. R. Birkelund, W. U. Schröder, W. W. Wilcke, and H. J. Wollersheim, *Proceedings of the Europhysics Conference on the Dynamics of Heavy Ion Collisions,* edited by N. Cindro, R. A. Ricci, and W. Greiner (North-Holland, Amsterdam, 1981), p. 15; and (unpublished).

[23]R. Bock, Y. T. Chu, M. Dakowski, A. Gobbi, E. Grosse, A. Olmi, H. Sann, D. Schwalm, U. Lynen, W. Müller, S. Bjørnholm, H. E. Esbensen, W. Wölfli, and E. Morenzoni, Nucl. Phys. (to be published).

[24]J. R. Huizenga, J. R. Birkelund, W. U. Schröder, and W. W. Wilcke, Nucl. Phys. (to be published).

[25]R. Bass, Nucl. Phys. A231, 45 (1974).

[26]K. L. Wolf, J. P. Unik, V. E. Viola, Jr., J. R. Birkelund, W. U. Schröder, H. Freiesleben, and J. R. Huizenga (unpublished).

[27]W. J. Swiatecki, Nucl. Phys. A376, 275 (1982).

[28]P. Dyer, R. J. Puigh, R. Vandenbosch, T. D. Thomas, and M. S. Zisman, Phys. Rev. Lett. 39, 392 (1977).

[29]J. Blocki, J. Randrup, W. J. Swiatecki, and C. F. Tsang, Ann. Phys. (N.Y.) 105, 427 (1977).

[30]W. U. Schröder, J. R. Birkelund, J. R. Huizenga, K. L. Wolf, J. P. Unik, and V. E. Viola, Jr., Phys. Rev. Lett. 36, 514 (1976).

[31]W. U. Schröder, J. R. Huizenga, J. R. Birkelund, K. L. Wolf, and V. E. Viola, Phys. Lett. 71B, 283 (1977).

[32]W. U. Schröder, J. R. Birkelund, J. R. Huizenga, K. L. Wolf, and V. E. Viola, Jr., Phys. Rep. 45, 301 (1978).

[33]W. U. Schröder, J. R. Birkelund, J. R. Huizenga, W. W. Wilcke, and J. Randrup, Phys. Rev. Lett. 44, 308 (1980).

[34]J. Randrup, Nucl. Phys. A307, 319 (1978).

[35]J. Randrup, Nucl. Phys. A327, 490 (1979).

[36]P. Dyer, M. P. Webb, R. J. Puigh, R. Vandenbosch, T. D. Thomas, and M. S. Zisman, Phys. Rev. C 22, 1509 (1980).

[37]S. S. Kapoor and J. N. De, Phys. Rev. C 26, 172 (1982).
[38]W. Nörenberg, Phys. Lett. 52B, 289 (1974).
[39]W. Nörenberg, Z. Phys. A 274, 241 (1975).
[40]W. U. Schröder, J. R. Huizenga, and J. Randrup, Phys. Lett. 98B, 355 (1981).
[41]W. J. Swiatecki, Lawrence Berkeley Laboratory Report LBL-8950, 1979.
[42]J. Blocki and W. J. Swiatecki, Ann. Phys. (N.Y.) 132, 53 (1981).
[43]W. U. Schröder and J. R. Huizenga, Comments Nucl. Part. Phys. 10, 19 (1981).
[44]J. Randrup, Nucl. Phys. A259, 253 (1976).
[45]J. Randrup, Nucl. Instrum. Methods 146, 213 (1977).
[46]J. P. Bondorf, M. I. Sobel, and D. Sperber, Phys. Rep. 45, 83 (1974).
[47]J. R. Birkelund, L. E. Tubbs, J. R. Huizenga, J. N. De, and D. Sperber, Phys. Rep. 56, 107 (1979).